

Strong Geometrical Dependence of the Absorption of Light in Arrays of Semiconductor Nanowires

Silke L. Diedenhofen,[†] Olaf T. A. Janssen,[‡] Grzegorz Grzela,[†] Erik P. A. M. Bakkers,^{§,⊥,||} and Jaime Gómez Rivas^{†,§,*}

[†]FOM Insitute AMOLF, c/o Philips Research Laboratories Eindhoven, High Tech Campus 4, 5656 AE Eindhoven, The Netherlands, [‡]Optics Research Group, Delft University of Technology, P.O. Box 5046, 2608 GA Delft, The Netherlands, [§]Applied Physics, Photonics & Semiconductor Nanophysics, Eindhoven University of Technology, 5600 MB Eindhoven, The Netherlands, [⊥]Kavli Institute of Nanoscience, Quantum Transport, Delft University of Technology, 2600 GA Delft, The Netherlands, and ^{||}Philips Research Laboratories, 5656 AE Eindhoven, The Netherlands

Advances in nanostructuring techniques have resulted in an increased interest of enhancing absorption in photovoltaic cells by means of nanostructures.^{1–15} Increasing absorption is of great importance to improve the performance and reduce the cost of photovoltaic cells, as it allows for the reduction of the active material while maintaining efficiency, at least from the optical point of view. In the race toward the realization of the perfect absorber, semiconductor nanowires are promising building blocks.¹⁶ Semiconductor nanowires have demonstrated their potential for next generation solar cells.^{1–4,9,14} Bottom-up growth techniques allow for the fabrication of nanowires heteroepitaxially and the control of the doping composition and concentration radially and axially.^{17–19} Photosensitive devices based on single nanowires and ensembles of nanowires have been demonstrated recently.^{1–5} Ensembles of nanowires are studied in relation to photovoltaics using different approaches. On the one hand, dense ensembles of nanowires forming graded refractive index layers can be used as an anti-reflecting layer to couple light very efficiently into high index semiconductors.^{6–8} On the other hand, the strong interaction of nanowires with light can be utilized to enhance the absorption in the nanowire layer. Random ensembles of vertically aligned nanowires have been demonstrated as efficient absorber material due to a reduction of specular reflectance at the interface and an increase of the optical path length in the nanowire layer by multiple scattering.¹¹ Solar cells based on random ensembles of non-epitaxially grown Si nanowires have been

ABSTRACT We demonstrate experimentally that arrays of base-tapered InP nanowires on top of an InP substrate form a broad band and omnidirectional absorbing medium. These characteristics are due to the specific geometry of the nanowires. Almost perfect absorption of light (higher than 97%) occurs in the system. We describe the strong optical absorption by finite-difference time-domain simulations and present the first study of the influence of the geometry of the nanowires on the enhancement of the optical absorption by arrays. Cylindrical nanowires present the highest absorption normalized to the volume fraction of the semiconductor. The absolute absorption in layers of conical nanowires is higher than that in cylindrical nanowires but requires a larger volume fraction of semiconducting material. Base-tapered nanowires, with a cylindrical top and a conical base, represent an intermediate geometry. These results set the basis for an optimized optical design of nanowire solar cells.

KEYWORDS: semiconductor nanowires · light management · optical absorption · anti-reflection · photovoltaics

reported with a peak external quantum efficiency of 12%.⁴ Several theoretical works have addressed the dependence of the absorption in arrays of semiconductor nanowires on the diameter of the nanowires or on the pitch of the array.^{20–24} Ordered arrays of dual-diameter nanopillars¹² and crystalline core/amorphous shell nanoneedle arrays¹³ have been presented for increasing absorption in Ge. However, in most works, the absorption has been overestimated because of experimental limitations in the detection of the diffusely reflected light.^{12,13,15} In the view of these previous results, the geometry of the nanowires influences the absorption of light in arrays of these nanostructures.¹⁶

In this article, we investigate theoretically the light absorption in arrays of three different nanowire geometries, namely, cylindrical nanowires, conical nanowires, and a combination of the previous structures in

* Address correspondence to rivas@amolf.nl.

Received for review December 25, 2010 and accepted February 21, 2011.

Published online March 02, 2011
10.1021/nn103596n

© 2011 American Chemical Society

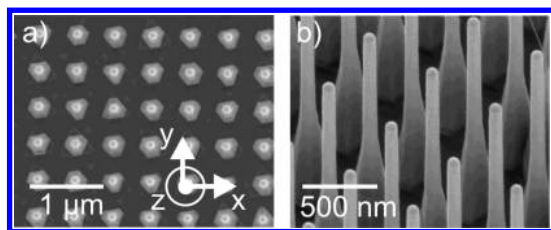


Figure 1. Scanning electron micrographs of arrays of InP nanowires. (a) Top-view, (b) tilted-view taken under an angle of 30° with respect to the nanowire elongation.

the form of nanowires with a cylindrical top and a tapered base. In the following, we will call the former geometry base-tapered nanowire. We find that the absorption is the highest in layers of conical nanowires, while the absorption relative to the volume fraction of the semiconductor is the highest in layers of cylindrical nanowires. Due to the broader base in conical nanowires, the amount of semiconductor is larger for this geometry. These findings indicate that, when the amount of material needs to be reduced, cylindrical wires perform best; however, if high absorption is required, independent of the material volume fraction, conical nanowires give the best result.

We have also investigated experimentally the absorption in the intermediate geometry, that is, base-tapered nanowires, by measuring the diffuse and specular reflection of InP base-tapered nanowire arrays on top of an InP substrate. Our results indicate a broad band and omnidirectional enhanced optical absorption in these arrays, with an absorption higher than 97.5% in the combined system of nanowires and substrate for wavelengths in the range of 400–850 nm. The absorption in the nanowire layer alone is on the order of 80%, while the additional absorption takes place in the substrate. These results demonstrate that it is possible to unify the strong light–nanowire interaction and the anti-reflection concepts by designing a layer of nanowires with a tapered base. Broad band and omnidirectional enhanced absorption are two of the required characteristics for improving the efficiency of solar cells.

RESULTS AND DISCUSSION

We have grown large-area arrays of InP nanowires on (111)B InP substrates using the vapor–liquid–solid (VLS) growth mechanism by metal–organic vapor phase epitaxy (MOVPE).²⁵ Details on the growth are given in the Methods and in ref 26. We have chosen to work with InP nanowires, as the electronic band gap energy of 1.344 eV ($\lambda_g = 922$ nm) allows for absorption in the visible and near-infrared, where the solar irradiance is high. InP is a direct band gap semiconductor with strong optical absorption in thin layers, which is commonly used in photovoltaic cells.²⁷ Figure 1 displays scanning electron micrographs (SEM) of arrays of InP nanowires. The top-view image (Figure 1a) shows

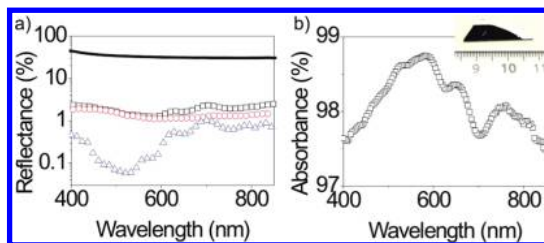


Figure 2. (a) Measured total reflectance (black squares), nonspecular reflectance (red circles), and specular reflectance (blue triangles) of the InP nanowire sample as a function of wavelength for an angle of incidence of 8° . The solid curve shows the measured total reflectance of bulk InP. (b) Measured absorbance in the InP nanowire sample. The inset in (b) shows a photograph of the nanowire sample. The region covered with nanowires is black, indicating high absorption. No nanowires are grown on the side of the sample, and the shiny InP substrate is visible.

that the nanowires are grown in a square lattice with a pitch of 513 nm. The hexagonal shape of the nanowires indicates the crystallographic structure of the nanowires. The crystallographic lattice is further studied by high-resolution transmission electron micrographs (see Supporting Information, Figure S1), revealing that this lattice is wurtzite. From the tilted-view SEM images (Figure 1b), the geometrical structure of the nanowires can be deduced. Due to epitaxial and preferred nanowire growth in the $\langle 111 \rangle$ direction,²⁸ the nanowires are vertically aligned. The total length of the nanowires is $3 \mu\text{m}$ with a straight top part with a length of $\sim 2 \mu\text{m}$ and a diameter of 90 ± 5 nm, and a tapered lower part with a length of $\sim 1 \mu\text{m}$. The diameter of the nanowires at the bottom is 270 ± 20 nm. The tapering of the nanowires results in an increase of InP filling fraction from around 2.3% at the top to 21% at the bottom. The tapering of the bottom section of the nanowires occurs intrinsically during the growth of the nanowires. We attribute this tapering to a short surface diffusion length of the precursors, which is induced by a high-temperature annealing step before the growth of the wires. By counting the missing wires in a low-magnification SEM image (Supporting Information, Figure S2a), the defect rate of the array can be estimated to be as low as 2.3%.

For determining the total absorbance in the InP, we have measured the angle-integrated or total reflectance of the nanowire layer for wavelengths between 400 and 850 nm and an angle of incidence of 8° . The experimental details are given in the Methods. The measurements (Figure 2a, black squares) show an overall reduction of the total reflectance with respect to a bulk InP substrate (black curve in Figure 2a). While the bulk InP substrate reflects more than 30% of the incident light, the reflectance of the base-tapered nanowire layer is lower than 2.5% over a broad wavelength range with a minimum of 1.25% at a wavelength of 580 nm. Additionally, we have measured the nonspecular reflectance of the nanowire array (red circles in Figure 2a). The difference of the total and

the nonspecular reflectance measurement provides the zero-order or the specular reflectance (blue triangles in Figure 2a). The specular reflectance achieves values as low as 0.05% at a wavelength around 510 nm. The nonspecular reflectance for the wavelength range between 400 and 600 nm can be attributed to diffraction of the incident light into higher reflection orders due to the regular nanowire pattern and to diffuse reflection due to defects in the array.

Because InP absorbs in the measured wavelength range, and as the InP nanowires are grown on top of a 300 μm thick InP substrate, we can assume a negligible transmission through the sample. Using this assumption, we can determine the total absorbance (TA) of the sample, that is, nanowire layer and substrate, by $\text{TA}(\%) = 100\% - \text{TR}(\%)$, with TR the measured total reflectance. The total absorbance is displayed in Figure 2b, and it is higher than 97.5% for all wavelengths with a maximum of 98.7% at 580 nm. The inset in Figure 2b shows a photograph of the base-tapered InP nanowire sample. The region covered with nanowires is indeed black as a result of the large absorption. The shiny, high reflecting InP substrate is visible at the edge, where no nanowires are grown. Note that if the absorption would have been determined from the specular reflectance measurements, it would have been overestimated to a maximum of 99.95% at 510 nm.

To study the low reflection of nanowire arrays in more detail for a wide range of angles, we have measured the angle-resolved specular reflectance for angles of incidence from 6 to 60°. While we focus here on the s-polarized reflectance, that is, polarization along the y-direction as defined in Figure 1, we have measured for p-polarized incident light a comparable ultralow specular reflectance. Figure 3a shows the measured specular reflectance as a function of wavelength at an angle of incidence of 8°. The measured specular reflectance is very low for all wavelengths, and Fabry-Pérot oscillations are visible due to the finite thickness of the nanowire layer. Surprisingly, the reflectance is also very low in the wavelength range between 900 and 1000 nm. Considering that the energy of photons in this wavelength range is lower than the electronic band gap of InP, the low reflection cannot be attributed to absorption but to an increased transmission into the substrate. In the following, we describe the measurements using transfer-matrix calculations.

We have performed transfer-matrix calculations²⁹ of a 4-layer system consisting of air, the straight part of the nanowires, the tapered part of the nanowires with a graded refractive index, and the InP substrate. These calculations, which are used to fit the Fabry-Pérot oscillations in the specular reflectance spectra, assume that the nanowire layer is a homogeneous medium in which the incident light is refracted due to the layer's effective refractive index and its intensity is reduced due to absorption and scattering. For modeling, the

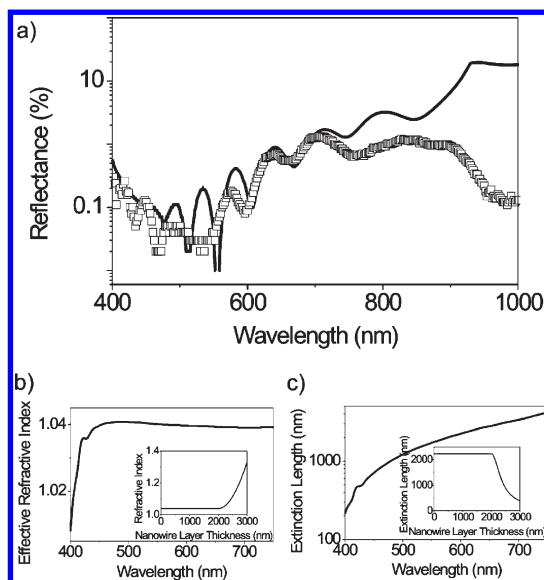


Figure 3. (a) Measurement of the specular reflectance (black squares) and calculation using a transfer-matrix method (black solid curve) at an angle of incidence of 8°. (b) Effective refractive index and (c) extinction length of the straight part of the InP nanowire layer obtained from fits of the transfer-matrix method to the measurements. The real part of the refractive index is close to unity in the whole spectral range. The extinction length increases with wavelength due to the reduction of the absorption and scattering by the InP nanowires. The insets in (b) and (c) show the effective refractive index and the effective extinction length as a function of nanowire layer thickness at 600 nm.

tapered part of the nanowire layer, this part was divided into sublayers with a thickness of 20 nm and a gradually increasing effective refractive index and effective extinction coefficient.⁶ The refractive indices of the straight and tapered part of the nanowires are obtained by fitting the period of the Fabry-Pérot oscillations, while the extinction coefficients of the straight and tapered part, characterizing the absorption and scattering, are obtained from the intensity of the reflectance. Figure 3a shows the measured specular reflectance (symbols) for an angle of incidence of 8° together with the calculated specular reflectance (curve) using the transfer-matrix method. The effective refractive index of the straight part of the nanowires layer and the extinction length, defined as $\lambda/(4\pi k_{\text{eff}})$, where k_{eff} is the extinction coefficient, are displayed in Figure 3b,c, respectively. The effective refractive index is lower than 1.04 over the measured wavelength range, resulting in nearly perfect optical matching at the interface of the nanowire layer with air and very efficient coupling of light into the nanowire layer. The inset in Figure 3b displays the refractive index as a function of nanowire layer thickness at a wavelength of 600 nm. The refractive index is increasing parabolically along the tapered part of the nanowire layer due to a parabolically increasing InP filling fraction in the layer. The effective extinction length (Figure 3c) increases with wavelength because of a decrease of the absorption and

scattering of the InP nanowires. The inset in Figure 3c displays the effective extinction length at a wavelength of 600 nm as a function of nanowire layer thickness. The effective extinction length is decreasing in the tapered part of the nanowire layer, as absorption is increasing due to an increasing InP filling fraction. For wavelengths longer than 800 nm, the transfer-matrix method fails in describing the measurement and the low specular reflectance for wavelengths between 900 and 1000 nm is not reproduced in the calculation. The disagreement at long wavelengths between the measurement and the transfer-matrix calculation is, as we will show later, due to the coupling of the incident light into guided modes supported by the tapered part of the nanowires. This coupling cannot be taken into account by the effective medium used in the transfer-matrix model.

Figure 4a shows the measurement of the specular reflectance for s-polarized incident light as a function of the angle of incidence and wavelength. The reflectance is very low over the whole spectral and angular range, with a maximum reflectance of 4% at 40° and 650 nm. The reflectance shows Fabry-Pérot oscillations due to the finite thickness of the nanowire layer. The reflectance is also very low for all angles in the wavelength range between 900 and 1000 nm. In the following, we describe the measurements using finite-difference time-domain (FDTD) simulations.

To understand the effect of the base-tapered nanowire geometry on the specular reflectance, we have performed FDTD simulations³⁰ of the reflectance of the nanowire layer. The FDTD simulation of the specular reflectance as a function of wavelength and angle of incidence is shown in Figure 4b for s-polarized incident light, that is, polarization along the *y*-direction as displayed in Figure 1a. A good qualitative agreement between measurements and simulations is obtained, reproducing the Fabry-Pérot oscillations, the low reflectance in the wavelength range between 900 and 1000 nm, and the band of higher reflection for angles of incidence between 20 and 55° and wavelengths between 450 and 800 nm. This band can be attributed to the periodicity of the nanowire array as FDTD simulations for different nanowire periods (not shown here) show a shift of the band. The small qualitative differences between measurement and FDTD simulation can be assigned to the following reasons: (i) The values of complex permittivity of InP used in the simulations are those of zinc blende InP,³¹ while the nanowires grow with wurtzite structure.³² Values of the permittivity of wurtzite InP are not reported in literature. (ii) The minor disorder of the nanowire layer, which is not included in the simulations, gives rise to nonspecular reflection (see Figure 2), resulting in a reduction of the measured specular reflection. (iii) The nanowires are approximated to a cylindrical shape with conical base, while the nanowires have a hexagonal shape. We have chosen this approximation because

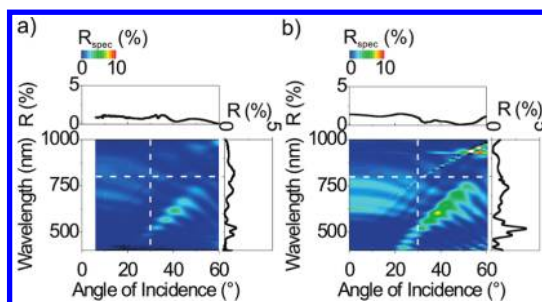


Figure 4. (a) Measured specular reflectance and (b) FDTD simulation of the specular reflectance of the base-tapered InP nanowire layer. The curves correspond to cuts along the dashed lines.

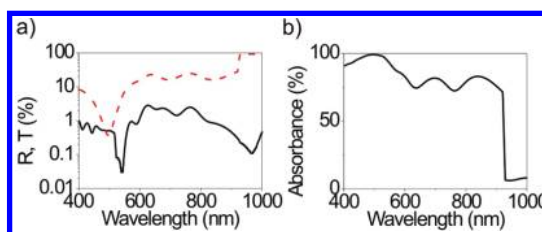


Figure 5. (a) Simulated angle-integrated reflectance (black solid curve) and transmittance (red dashed curve) of InP nanowires on top of a non-absorbing substrate at normal incidence. (b) Simulated absorbance of the nanowire layer. For wavelengths longer than 920 nm, at which InP does not absorb, more than 90% of the incident light is coupled into the underlying substrate. The calculated absorbance shows that around 80% of the incident light is absorbed by the base-tapered nanowire layer.

the hexagonal shape changes from nanowire to nanowire (see Figure 1). Considering that the geometry used in the FDTD simulations includes the periodicity of the base-tapered nanowires array, we can assume that the intensity of the diffracted light that is captured neither in the specular reflectance measurement nor in the FDTD simulation of the specular reflectance is similar. Therefore, we can assume that the minor discrepancy between the specular reflectance measurement and FDTD simulation is not due to diffraction.

Since we have performed measurements using InP nanowires grown on an InP substrate, we cannot conclude from the measurements if the strong absorbance and the reduced reflectance are solely due to enhanced absorption in the nanowire layer or also to enhanced light coupling into the substrate. Therefore, we have simulated the total reflectance using FDTD by assuming a substrate with an identical real part of the refractive index of InP, but by ignoring its absorption. In Figure 5a, we present the simulated total reflectance (black solid curve) and total transmittance (red dashed curve) of nanowires on top of a non-absorbing substrate. Fabry-Pérot oscillations are visible in both simulations. The pronounced dip in the reflectance at a wavelength of 540 nm is due to the Rayleigh anomaly, that is, the angle and wavelength at which a diffracted order of the structure becomes evanescent. The sharp increase of the transmittance at 920 nm is due to the

absence of absorption in the nanowire layer for wavelengths longer than the electronic band gap of InP. Figure 5b displays the absorbance in the nanowire layer obtained from the simulated reflectance and transmittance. We estimate from Figure 5b that around 80% of the light is absorbed by the base-tapered nanowire layer at wavelengths between 550 and 900 nm and more than 90% is absorbed for shorter wavelengths. For wavelengths longer than the electronic band gap, the absorption drops to very low values. This residual absorption in the simulation is due to the definition of the material constants in the FDTD simulation.

To better understand the origin of the measured reflectance, it is worth to look at the electric field distribution around the nanowires. Therefore, we determine the dominant component of the electric field, that is, the y -component. This component is oriented parallel to the polarization vector of the incident wave, and its orientation with respect to the nanowire geometry is displayed in Figure 1a. These simulations are presented in Figure 6, where the electric and displacement field are plotted for an angle of incidence of 40° and at four different wavelengths, namely, 505 nm (Figure 6a,e), 605 nm (Figure 6b,f), 688 nm (Figure 6c,g), and 980 nm (Figure 6d,h). The displacement field is useful to visualize the field inside the nanowires, as this field is magnified by a factor given by the permittivity of InP. At 505 nm (Figure 6a), InP absorbs strongly and the electric field does not reach the substrate. At this wavelength, the displacement field is concentrated at the top of the wire (Figure 6e), indicating that most of the absorption occurs at the top. From the equal tilt of the wavefront above and inside the nanowire layer, we can conclude that the light is transmitted into the layer with negligible refraction. This absence of refraction confirms that the nanowire layer has a low effective refractive index with a value close to 1, as it was determined from the transfer-matrix fits to the measurements. The combination of strong absorption and low refraction explains the low reflectance of the sample at short wavelengths. At 605 nm (Figure 6b) and 688 nm (Figure 6c), InP absorbs only moderately.³¹ The displacement field (Figure 6f,g) shows that next to some absorption in the straight part of the wire, the tapered region plays an important role in the high absorbance and low reflectance of the sample. Light is efficiently coupled to guided modes in the tapered InP region, resulting in high internal fields in this part of the nanowires. Below the band gap energy of InP, at a wavelength of 980 nm, there is no absorption. At this wavelength, the reflectance is remarkably low. The calculation of the fields (Figure 6d,h) reveals that the incident light couples very efficiently to the lowest order waveguide mode in the tapered region and is fully transmitted into the InP substrate. Therefore, from the near-field simulations, we can conclude that for short wavelengths light is absorbed in the straight part of the wires, while at longer wavelengths the tapering of the nanowires is essential for

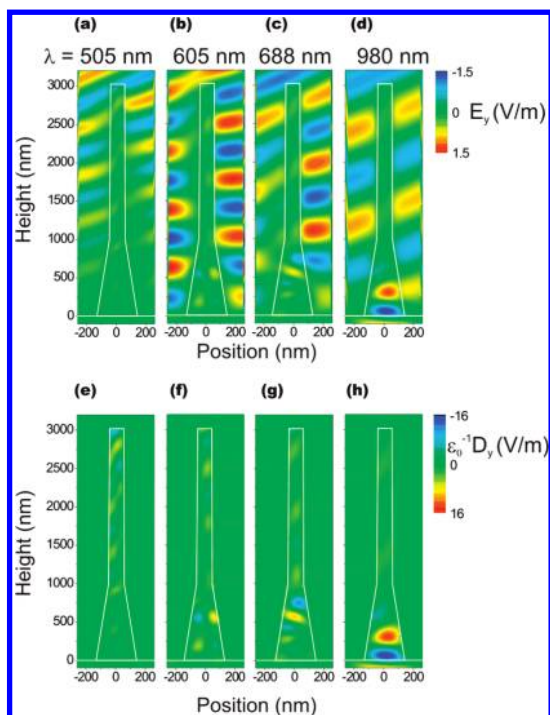


Figure 6. Simulated electric field amplitude and electric displacement field components along the y -direction in a plane along the nanowire axis for an angle of incidence of 40° and for wavelengths of 505 nm (a,e), 605 nm (b,f), 688 nm (c,g), and 980 nm (d,h). The incident field has an amplitude of 1 V/m.

strong absorption. In the wavelength range between 900 and 1000 nm, where a very low reflectance is measured, the incident light is guided efficiently into the substrate by the tapered section of the nanowires.

Comparison of Nanowire Geometry. Once we have established the relevance of the tapered section of the nanowires for the optical response of the layer, we compare the simulations of the absorbance of a layer of base-tapered, cylindrical, and conical nanowires for normal incidence (Figure 7a) and for an angle of incidence of 30° (Figure 7b). The cylindrical wires have a diameter of 90 nm and a length of $3 \mu\text{m}$. The conical nanowires have a top diameter of 90 nm, a bottom diameter of 270 nm and a height of $3 \mu\text{m}$. The base-tapered nanowires have the same geometry as before, that is, a straight top section with a length of $2 \mu\text{m}$ and a nanowire diameter of 90 nm, and a tapered bottom section with a length of $1 \mu\text{m}$. The bottom diameter of the base-tapered nanowires is 270 nm. Therefore, the length of the wires is kept constant for the three geometries.

For both angles of incidence and for wavelengths below 550 nm, the absorbance in the layer of cylindrical nanowires (red dashed curve), the layer of base-tapered nanowires (black solid curve), and the layer of conical nanowires (blue dashed dotted curve) are almost identical. Therefore, we can conclude that the geometry of the nanowires has a minor influence in the absorbance at these wavelengths. Note that the large

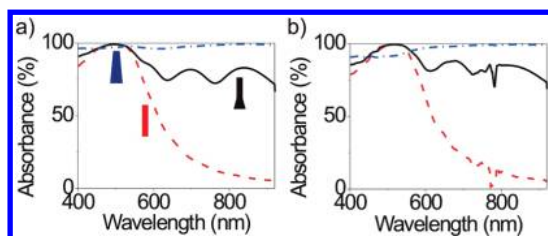


Figure 7. Simulated absorbance of base-tapered nanowires (black solid curve), cylindrical nanowires (red dashed curve), and conical nanowires (blue dashed-dotted curve) for (a) normal incidence and (b) an angle of incidence of 30° . The length of the nanowires is $3 \mu\text{m}$, and the nanowires' diameter at the top is 90 nm for the three geometries. The diameter at the bottom is 270 nm for the base-tapered and conical nanowires. The dips in the absorbance in (b) at 780 nm are a Rayleigh anomaly, or a diffracted order in the periodic structure becoming evanescent, at this particular wavelength and angle of incidence.

absorbance at short wavelengths agrees with the near-field data of Figure 6, where we found that most of the light is absorbed in the straight top part of the wires. As we can see in Figure 7a,b, for both angles of incidence and for longer wavelengths than 550 nm , the absorbance in the layer of base-tapered nanowires is strongly enhanced compared to the absorbance of the layer of cylindrical nanowires, and this absorbance is further enhanced in the layer of conical nanowires. At these wavelengths, light is absorbed by the tapered part, due to the higher material filling fraction and the coupling of light to guided modes in the nanowires.

From the simulated absorption of the three geometries displayed in Figure 7a,b, we can conclude that the absorption is the highest in the layer of conical nanowires. To quantify the difference in absorption in the three different layers, we have determined the averaged wavelength-integrated absorption at normal incidence for wavelengths between 400 and 920 nm in each nanowire layer. The averaged wavelength-integrated absorbances are 98 , 84 , and 45% in the layer of conical, base-tapered, and cylindrical nanowires, respectively. This difference in absorption can be attributed to differences in the geometry that change the coupling of light into the layer and to differences in the volume fraction of the semiconductor. These volume fractions are 0.104 , 0.051 , and 0.024 for the conical, base-tapered, and cylindrical nanowires, respectively. The averaged wavelength-integrated absorbances normalized to the volume fraction of semiconductor are 940 , 1647 , and 1875% for layers of conical, base-tapered, and

cylindrical nanowires. Therefore, cylindrical nanowires form the most efficient absorber medium relative to the amount of material.

These calculations provide the guidelines for the design of optically optimized nanowire based solar cells. In case that the absorption needs to be maximized, the best choice of geometry is conical nanowires. In case the semiconductor material needs to be reduced, the best geometry is cylindrical nanowires. This geometry provides a moderate absorption but requires only one-fourth of semiconductor compared to conical wires. A good compromise between these two geometries is base-tapered nanowires. The absorbance for the example of base-tapered nanowires described above is similar to that of conical nanowires, while only half of the material is required to achieve this absorption.

CONCLUSIONS

We have demonstrated enhanced broad band and omnidirectional absorbance in arrays of base-tapered InP nanowires grown by the vapor–liquid–solid mechanism on top of an InP substrate. Measurements of the total reflectance reveal that the optical absorbance in the nanowire layer and substrate is higher than 97% in the visible and near-infrared. The strong optical absorption is confirmed by finite-difference time-domain simulations. Different mechanisms are responsible for this absorption. First, the low effective refractive index of the nanowire layer allows for a nearly perfect coupling of the incident light into the layer. Second, the strong absorption in InP has a major role at short wavelengths, while for longer wavelengths, the light is efficiently coupled to guided modes in the tapered part of the nanowires. From the FDTD simulations, we determine that the absorption in the nanowire layer alone, that is, without considering the effect of the absorbing substrate, is larger than 80% . A comparison of the absorption in layers of cylindrical, base-tapered, and conical nanowires shows that the absorption is the highest in conical nanowires, but that cylindrical nanowires form the most efficient absorber medium when considering the amount of semiconductor. A similar absorption efficiency than in conical nanowires can be obtained with base-tapered nanowires with a significant lower amount of semiconductor. This investigation of the influence of the nanowire geometry on the absorption sets the basis for the optimization of nanowires based solar cells.

METHODS

VLS Growth. The VLS growth mechanism requires a metal catalyst particle. To achieve ordered arrays of nanowires, we have used substrate conformal imprint lithography (SCIL) for patterning gold. A detailed description of SCIL and the nanowire

growth process used can be found in ref 26. SCIL allows the fabrication of large-area arrays of nanowires in a low-cost process with a high reproducibility. The InP nanowires are grown for 60 min at a temperature of 420°C using trimethylindium (TMIn) and phosphine (PH₃) as precursors.

Total Reflectance Measurement. We measured the total reflectance of the layer of nanowires using a Lambda 950 spectrometer (PerkinElmer) consisting of a tungsten–halogen and a deuterium lamp, an integrating sphere, and a photomultiplier tube. For the reflectance measurements, the samples were mounted at the backside of the integrating sphere. The angle of incidence was 8°, allowing the measurement of the specularly and nonspecularly reflected light simultaneously. The nonspecularly reflected light is measured by making a small opening in the integrating sphere in such a way that the specularly reflected light escapes from the sphere. The reflection measurements on the nanowire arrays are normalized by the reflection of a white-standard to obtain the absolute reflectance of the array.

Angle-Resolved Specular Reflectance Measurement. For this measurement, the sample and detector are mounted on a set of computer-controlled rotation stages. The sample was illuminated using the collimated beam of a fiber-coupled supercontinuum light source (Fianium SC400-PP), and the spectra were obtained using a fiber-coupled Si spectrometer (Ocean Optics, USB2000) for the visible and a fiber-coupled InGaAs spectrometer (Andor iDus) for the near-infrared. A schematic of the experimental setup is given in Figure S3 (see Supporting Information).

FDTD Simulations. We have used an in-house developed FDTD program on a computational domain consisting of a nanowire on a semi-infinite substrate.³⁰ The domain has quasiperiodic boundary conditions³³ in the horizontal directions and absorbing perfectly matched layers (PML) boundaries³⁴ in the vertical directions. The dispersion of the permittivity of InP is taken into account by fitting the refractive index of zinc blende InP with a Lorentz model above and below the band gap.³¹ The spectral response of the nanowire layer is obtained by using a short 0.5 fs incident pulse with constant transverse wavenumber and Fourier transforming the simulated time-domain data. The reflectance and transmittance are computed from the fields in a plane above the nanowire and 50 nm in the substrate, respectively.

Acknowledgment. We thank A. Pierret, M. Hocevar, R. Algra, E. Timmering, M. Verschuuren, and E. van Thiel for technical assistance, H. de Barse for SEM analysis, and M. Verheijen for TEM analysis, and M. Leistikow, S. Huismans, and W. Vos for useful discussions. This work is part of the research program of the “Stichting voor Fundamenteel Onderzoek der Materie (FOM)”, which is financially supported by the “Nederlandse organisatie voor Wetenschappelijk Onderzoek (NWO)” and is part of an industrial partnership program between Philips and FOM. This research is supported by the Dutch Technology Foundation STW, which is the applied science division of NWO, and the Technology Programme of the Ministry of Economic Affairs (project number 10301).

Supporting Information Available: The contents of the Supporting Information include the following: (1) TEM images of an individual nanowire, (2) SEM images of the array of base-tapered nanowires, (3) schematic representation of the specular reflection measurement setup. This material is available free of charge via the Internet at <http://pubs.acs.org>.

REFERENCES AND NOTES

- Tian, B.; Zheng, X.; Kempa, T. J.; Fang, Y.; Yu, N.; Yu, G.; Huang, J.; Lieber, C. M. Coaxial Silicon Nanowires as Solar Cells and Nanoelectronic Power Sources. *Nature* **2007**, *449*, 885–890.
- Goodey, A. P.; Eichfeld, S. M.; Lew, K.-K.; Redwing, J. M.; Mallouk, T. E. Silicon Nanowire Array Photoelectrochemical Cells. *J. Am. Chem. Soc.* **2007**, *129*, 12344–12345.
- Sivakov, V.; Andrä, G.; Gawlick, A.; Berger, A.; Plentz, J.; Falk, F.; Christiansen, S. H. Silicon Nanowire-Based Solar Cells on Glass: Synthesis, Optical Properties, and Cell Parameters. *Nano Lett.* **2009**, *9*, 1549–1554.
- Tsakalacos, L.; Balch, J.; Fronheiser, J.; Korevaar, B. A.; Sulima, O.; Rand, J. Silicon Nanowire Solar Cells. *Appl. Phys. Lett.* **2007**, *91*, 233117/1-3.

- Kelzenberg, M. D.; Boettcher, S. W.; Petykievicz, J. A.; Turner-Evans, D. B.; Puntam, M. C.; Warren, E. L.; Spurgeon, J. M.; Briggs, R. M.; Lewis, N. S.; Atwater, H. A. Enhanced Absorption and Carrier Collection in Si Wire Arrays for Photovoltaic Applications. *Nat. Mater.* **2010**, *9*, 205–213.
- Diedenhofen, S. L.; Vecchi, G.; Algra, R. E.; Hartsuiker, A.; Muskens, O. L.; Immink, G.; Bakkers, E. P. A. M.; Vos, W. L.; Gómez Rivas, J. Broad-Band and Omnidirectional Antireflection Coatings Based on Semiconductor Nanorods. *Adv. Mater.* **2009**, *21*, 973–978.
- Lee, Y.-J.; Ruby, D. S.; Peters, D. W.; McKenzie, B. B.; Hsu, J. W. P. ZnO Nanostructures as Efficient Antireflection Layers in Solar Cells. *Nano Lett.* **2008**, *8*, 1501–1505.
- Chattopadhyay, S.; Huang, Y. F.; Jen, A. J.; Ganguly, A.; Chen, K. H.; Chen, L. C. Anti-reflecting and Photonic Nanostructures. *Mater. Sci. Eng., R* **2010**, *69*, 1–35.
- Cao, L.; White, J. S.; Park, J.-S.; Schuller, J. A.; Clemens, B. M.; Brongersma, M. L. Engineering Light Absorption in Semiconductor Nanowire Devices. *Nat. Mater.* **2009**, *8*, 643–647.
- Wei, W.; Bao, X.-Y.; Soci, C.; Ding, Y.; Wang, Z.-L.; Wang, D. Direct Heteroepitaxy of Vertical InAs Nanowires on Si Substrates for Broad Band Photovoltaics and Photodetection. *Nano Lett.* **2009**, *9*, 2926–2934.
- Muskens, O. L.; Gómez Rivas, J.; Algra, R. E.; Bakkers, E. P. A. M.; Lagendijk, A. Designing Light Scattering in Nanowire Materials for Photovoltaic Applications. *Nano Lett.* **2008**, *8*, 2638–2642.
- Fan, Z.; Kapadia, R.; Leu, P. W.; Zhang, X.; Chueh, Y.-L.; Takei, K.; Yu, K.; Jamshidi, A.; Rathore, A. A.; Ruebusch, D. J.; Javey, A. Ordered Arrays of Dual-Diameter Nanopillars for Maximized Optical Absorption. *Nano Lett.* **2010**, *10*, 3823–3827.
- Chueh, Y.-L.; Fan, Z.; Takei, K.; Ko, H.; Kapadia, R.; Rathore, A. A.; Miller, N.; Yu, K.; Wu, M.; Haller, E. E.; Javey, A. Black Ge Based on Crystalline/Amorphous Core/Shell Nanoneedle Arrays. *Nano Lett.* **2010**, *10*, 520–523.
- Garnett, E.; Yang, P. Light Trapping in Silicon Nanowire Solar Cells. *Nano Lett.* **2010**, *10*, 1082–1087.
- Lu, Y.; Lal, A. High-Efficiency Ordered Silicon Nano-Conical-Frustum Array Solar Cells by Self-Powered Parallel Electron Lithography. *Nano Lett.* **2010**, *10*, 4651–4656.
- Zhu, J.; Yu, Z.; Fan, S.; Cui, Y. Nanostructured Photon Management for High Performance Solar Cells. *Mater. Sci. Eng., R* **2010**, *70*, 330–340.
- Bakkers, E. P. A. M.; van Dam, J. A.; Franceschi, S. D.; Kouwenhoven, L. P.; Kaiser, M.; Verheijen, M.; Wondergerm, H.; van der Sluis, P. Epitaxial Growth of InP Nanowires on Germanium. *Nat. Mater.* **2004**, *3*, 769–773.
- Haraguchi, K.; Katsuyama, T.; Hiruma, K.; Ogawa, K. GaAs p–n Junction Formed in Quantum Wire Crystals. *Appl. Phys. Lett.* **1992**, *60*, 745–747.
- Stiegler, J. M.; Huber, A. J.; Diedenhofen, S. L.; Gómez Rivas, J.; Algra, R. E.; Bakkers, E. P. A. M.; Hillenbrand, R. Nanoscale Free-Carrier Profiling of Individual Semiconductor Nanowires by Infrared Near-Field Nanoscopy. *Nano Lett.* **2010**, *10*, 1387–1392.
- Hu, L.; Chen, G. Analysis of Optical Absorption in Silicon Nanowire Arrays for Photovoltaic Applications. *Nano Lett.* **2007**, *7*, 3249–3252.
- Li, J.; Yu, H.; Wong, S. M.; Zhang, G.; Sun, X.; Lo, P. G.-Q.; Kwong, D.-L. Si Nanopillar Array Optimization on Si Thin Films for Solar Energy Harvesting. *Appl. Phys. Lett.* **2009**, *95*, 033102/1-3.
- Lin, C.; Povinelli, M. L. Optical Absorption Enhancement in Silicon Nanowire Arrays with a Large Lattice Constant for Photovoltaic Applications. *Opt. Express* **2009**, *17*, 19371–19381.
- Anttu, N.; Xu, H. Q. Coupling of Light into Nanowire Arrays and Subsequent Absorption. *J. Nanosci. Nanotechnol.* **2010**, *10*, 7183–7187.
- Kupec, J.; Witzigmann, B. Dispersion, Wave Propagation and Efficiency Analysis of Nanowire Solar Cells. *Opt. Express* **2009**, *17*, 10399–10410.

25. Wagner, R. S.; Ellis, W. C. Vapor–Liquid–Solid Mechanism of Single Crystal Growth. *Appl. Phys. Lett.* **1964**, *4*, 89–90.
26. Pierret, A.; Hocevar, M.; Diedenhofen, S. L.; Algra, R. E.; Vlieg, E.; Timmering, E. C.; Verschuuren, M. A.; Immink, G. W. G.; Verheijen, M. A.; Bakkers, E. P. A. M. Generic Nano-Imprint Process for Fabrication of Nanowire Arrays. *Nanotechnology* **2010**, *21*, 065305/1-6.
27. Spitzer, M. B.; Keavney, C. J.; Vernon, S. M.; Haven, V. E. Indium Phosphide Shallow Homojunction Solar Cells Made by Metalorganic Chemical Vapor Deposition. *Appl. Phys. Lett.* **1987**, *51*, 364/1-3.
28. Wacaser, B. A.; Dick, K. A.; Johansson, J.; Borgström, M. T.; Deppert, K.; Samuelson, L. Preferential Interface Nucleation: An Expansion of the VLS Growth Mechanism for Nanowires. *Adv. Mater.* **2009**, *21*, 153–165.
29. Yeh, P. *Optical Waves in Layered Media*; John Wiley and Sons: New York, 1988.
30. Besbes, M.; Hugonin, J. P.; Lalanne, P.; van Haver, S.; Janssen, O. T. A.; Nugrowati, A. M.; Xu, M.; Pereira, S. F.; Urbach, H. P.; van de Nes, A. S.; *et al.* Numerical Analysis of a Slit-Groove Diffraction Problem. *J. Eur. Opt. Soc.* **2007**, *2*, 07022/1-17.
31. Palik, E. D. *Handbook of Optical Constants of Solids*; Academic Press: San Diego, CA, 1998.
32. The optical constants of wurtzite InP are not reported in literature. Although we do not expect a large difference in these constants with respect to zinc blende InP, small variations are possible.
33. Aminian, A.; Rahmat-Samii, Y. Spectral FDTD: A Novel Technique for the Analysis of Oblique Incident Plane Wave on Periodic Structures. *IEEE Trans. Antennas Prop.* **2006**, *54*, 1818–1825.
34. Roden, J. A.; Gedney, S. D. Convolutional PML (CPML): An Efficient FDTD Implementation of the CFS-PML for Arbitrary Media. *Microwave Opt. Technol. Lett.* **2000**, *27*, 334–339.